Accuracy and stability analysis of the Semi-Lagrangian method for stiff hyperbolic relaxation systems and kinetic BGK model

Mingchang Ding [1] , Jing-Mei Qiu [2] , Ruiwen Shu [3]

Abstract

In this paper, we develop a family of third order asymptotic-preserving (AP) and asymptotically accurate (AA) diagonally implicit Runge-Kutta (DIRK) time discretization methods for the stiff hyperbolic relaxation systems and kinetic Bhatnagar-Gross-Krook (BGK) model in the semi-Lagrangian (SL) setting. The methods are constructed based on an accuracy analysis of the SL scheme for stiff hyperbolic relaxation systems and kinetic BGK model in the limiting fluid regime when the Knudsen number approaches 0. An extra order condition for the asymptotic third order accuracy in the limiting regime is derived. Linear von Neumann stability analysis of the proposed third order DIRK methods are performed to a simplified two-velocity linear kinetic model. Extensive numerical tests are presented to demonstrate the AA, AP and stability properties of our proposed schemes.

Keywords: Hyperbolic relaxation system; BGK model; semi-Lagrangian (SL) method; diagonally implicit Runge-Kutta (DIRK) method; asymptotic-preserving; asymptotic accuracy, von Neumann analysis.

1. Introduction. The models of interests in this paper include stiff hyperbolic relaxation models and the BGK model, the latter of which was introduced by Bhatnagar, Gross and Krook [4] as a relaxation model for the Boltzmann equation. In these models, a stiffness parameter ϵ characterizes multi-scale regime of the model. For example, in the BGK model, ϵ is the dimensionless Knudsen number, defined as $\epsilon = \lambda/L$ with mean free path λ and macroscopic characteristic length L. The BGK

[1]Computational Mathematics Science and Engineering, Michigan State University, East Lansing, MI 48824, USA. E-mail: dingmin2@msu.edu.

[2]Department of Mathematical Sciences, University of Delaware, Newark, DE, 19716, USA. E-mail: jingqiu@udel.edu. Research of the first and second author is supported by NSF grant NSF-DMS-1834686 and NSF-DMS-1818924 (Program manager: Dr. Leland M. Jameson), Air Force Office of Scientific Research FA9550-18-1-0257 (Program manager: Dr. Fariba Fahroo).

[3]Department of Mathematics, University of Maryland, College Park, MD, 20742, USA. E-mail: rshu@cscamm.umd.edu

model is in the kinetic regime with $\epsilon = O(1)$ for rarefied gas, and is in the hydrodynamic regime with $\epsilon \ll 1$. In the hydrodynamic regime, the BGK model gives a macroscopic model such as the Euler system as ϵ approaches 0, by the classical Champan-Enskog expansion [8, 11]. In this paper, we consider development of high order asymptotic preserving (AP) and asymptotic accurate (AA) numerical methods for the above mentioned multi-scale models.

Due to the stiffness of the collision term, an explicit time discretization would require the time step Δt to be $O(\epsilon)$, which is very expensive if ϵ is small. To avoid this time step restriction, people prefer to use AP schemes [24] which automatically become consistent numerical methods for the limiting macroscopic model as $\epsilon \to 0$. As a result, one can take Δt independent of ϵ, and the computational cost is dramatically decreased in the hydrodynamic regime, compared to explicit schemes. One also prefers schemes with the AA property, meaning that the scheme remains its optimal order in the hydrodynamic regime. High order AP / AA schemes for hyperbolic relaxation models and stiff kinetic equations have been developed based on various frameworks, such as implicit-explicit (IMEX) Runge-Kutta (RK) methods [23, 25, 3, 28, 29, 16, 13, 20], IMEX-multistep methods [2, 22, 14, 1], exponential-RK methods [12, 26, 21, 18] and semi-Lagrangian methods [30, 17, 5].

For transport problems, the semi-Lagrangian (SL) method is often designed via tracking solutions along characteristics of transport terms in time, thus easing the classical time step restrictions. Because of its computational efficiency due to large time stepping sizes, the SL method is popular in climate modeling [27, 33] and plasma simulations [32]. When handling source/diffusion/relaxation terms in the SL framework, these terms are often integrated in time along characteristics by explicit, implicit or IMEX RK or multistep type time integrators. Yet, study on asymptotic accuracy of the high order time integrator in the SL framework when applied to stiff hyperbolic systems is still lacking. In fact, it is numerically observed that a third order diagonally implicit RK (DIRK) method, when applied in the SL framework, suffers from accuracy degeneracy, with only second order temporal convergence observed in the asymptotic limit, see in [30].

In this paper, our first goal is to study the order reduction phenomenon in the

limiting regime. In particular, we conduct the accuracy analysis of DIRK methods for both kinetic and fluid regimes in the SL setting. Our accuracy analysis is semi-discrete in the sense that we only discretize in time, but keep the spatial operations at the continuous level. From the accuracy analysis, we find that the traditional order conditions of first order backward Euler method and second order DIRK (DIRK2) method [3] still hold in both the kinetic and fluid regimes, while one extra order condition needs to be imposed to ensure the third order accuracy in the limiting fluid regime. Taking this observation into consideration, we construct several new DIRK3 methods. We also study linear stability of high order DIRK schemes, in the SL framework, by performing the von Neumann analysis to a linear two-velocity kinetic model with relaxation term, from which we choose a third order accurate DIRK method in both kinetic and fluid regimes and with best linear stability property and robustness. There are open issues remain to be addressed in the future work: one is to optimize the stability property of AA DIRK3 methods in the SL framework; another is that our current stability analysis is performed in the semi-discrete sense with spatial operations kept at continuous level. Fully discrete stability analysis is very involved, especially with the change of stencil around the feet of characteristics when time stepping sizes are larger than the CFL limit. In fact, numerical instability is observed for the linear two-velocity model when the time stepping size is larger than CFL limit; while high order temporal convergence is observed for the nonlinear BGK model with large time stepping sizes.

The rest of the paper is organized as follows. In Section 2, we introduce our models of interests, i.e. the stiff hyperbolic relaxation systems and the BGK model. In Section 3, the SL scheme using DIRK for integration of stiff relaxation terms along characteristics is introduced. Section 3.2 is devoted to the accuracy analysis of the DIRK methods, integrating along characteristics, in the limiting fluid regime. In particular, an extra order condition for third order DIRK schemes is derived and new Butcher tableaus are constructed accordingly. The linear stability of DIRK methods is studied in Section 4. In Section 5, we show the asymptotic accuracy and stability property of DIRK schemes, when coupled with SL methods, via several stiff hyperbolic relaxation models. Conclusions are given in Section 6.

2. Stiff hyperbolic relaxation systems and BGK model. We consider

$$\partial_t f + v \cdot \nabla_x f = \frac{1}{\epsilon}\mathcal{Q}(f), \tag{2.1}$$

where $f = f(x, v, t)$ is the probability density function (PDF) of particles that depends on time t, position $x \in \Omega_x$ and velocity $v \in \Omega_v$, $\epsilon > 0$ is a dimensionless parameter. $\mathcal{Q}(f)$ is the relaxation operator that describes the interactions between particles. In particular, $\mathcal{Q}$ could be linear/nonlinear stiff relaxation terms for the following cases:

- Linear two-velocity model[4]

$$\begin{cases} \partial_t f_1 + \partial_x f_1 = \frac{1}{2\epsilon}(b(f_1 + f_2) - (f_1 - f_2)) \\ \partial_t f_2 - \partial_x f_2 = -\frac{1}{2\epsilon}(b(f_1 + f_2) - (f_1 - f_2)) \end{cases}. \tag{2.2}$$

  where $|b| < 1$ is a constant. (2.2) can be further written into

$$\partial_t f + v\partial_x f = \frac{1}{\epsilon}\mathcal{Q}(f) \tag{2.3}$$

  of the same form as (2.1). Here $v \in \Omega_v = \{1, -1\}$ with equal integration weights, $f(t, x, \cdot) = (f_1, f_2)^T$ and the collision operator

$$\mathcal{Q}(f) = \begin{pmatrix} \frac{1}{2}(b(f_1 + f_2) - (f_1 - f_2)) \\ -\frac{1}{2}(b(f_1 + f_2) - (f_1 - f_2)) \end{pmatrix}. \tag{2.4}$$

  When $\mathcal{Q}(f) = 0$, the equilibrium $M_U(t, x) = (M_1, M_2)^T$ is

$$f = M_U = \begin{pmatrix} \frac{1+b}{2}U \\ \frac{1-b}{2}U \end{pmatrix}, \quad U = \langle f\phi \rangle = f_1 + f_2 \tag{2.5}$$

  with one collision invariant

$$\phi = \phi(v) := 1, \quad \langle g \rangle := \sum_{v \in \Omega_v} g(v). \tag{2.6}$$

  When $\epsilon \to 0$, the limit of (2.2) is the linear transport equation $\partial_t u + b\partial_x u = 0$.

- The considered BGK model

$$\partial_t f + v \cdot \nabla_x f = \frac{1}{\epsilon}(M_U - f) \tag{2.7}$$

[4]This is indeed the same model as eq. (1.1) of [19] under the change of variable $f_1 = \frac{u+v}{2}$, $f_2 = \frac{u-v}{2}$.

where $f = f(x, v, t)$ is the distribution function of particles that depends on time $t > 0$, position $x \in \Omega_x$ and velocity $v \in \mathbb{R}^d$ with $d \geq 1$. Note that the BGK model is also of form (2.1) if $\mathcal{Q}(f) = M_U - f$. M_U is the local Maxwellian defined by

$$M_U = M_U(x, v, t) = \frac{\rho(x,t)}{(2\pi T(x,t))^{d/2}} \exp\left(-\frac{|v - u(x,t)|^2}{2T(x,t)}\right) \tag{2.8}$$

where ρ, u, T represent the macroscopic density, the mean velocity and the temperature respectively. They are computed by

$$\rho = \int_{\mathbb{R}^d} f \, dv, \quad u = \frac{1}{\rho}\int_{\mathbb{R}^d} f \cdot v \, dv, \quad T = \frac{1}{d\rho}\int_{\mathbb{R}^d} f|v - u|^2 \, dv.$$

The macroscopic fields U with the components of the density, momentum and energy is obtained by taking the first few moments of f:

$$U := (\rho, \rho u, E)^\top = \langle f\phi \rangle \tag{2.9}$$

with

$$\phi = \phi(v) := \left(1, v, \frac{1}{2}|v|^2\right)^\top, \quad \langle g \rangle := \int_{\mathbb{R}^d} g(v) dv. \tag{2.10}$$

The total energy E is related to T through $E = \frac{1}{2}\rho|u|^2 + \frac{d}{2}\rho T$. It is easy to check that $\langle M_U \phi \rangle = U$. Hence with (2.9), we see that

$$\langle (M_U - f)\phi \rangle = 0, \tag{2.11}$$

namely the BGK operator satisfies the conservation of mass, momentum and energy. Moreover, it enjoys the entropy dissipation: $\langle (M_U - f) \log f \rangle \leq 0$. See [10, 8, 9] for more details of the BGK model.

We rewrite the general stiff relaxation equation (2.1)

$$\partial_t f + v \cdot \nabla_x f = \frac{1}{\epsilon}\mathcal{Q}(f), \tag{2.12}$$

where $\mathcal{Q}(f)$ satisfies the following properties:

- Collision invariants: there exists $\phi(v) := (\phi_1(v), \dots \phi_K(v))^T$ such that

$$\langle \mathcal{Q}(f)\phi \rangle = 0, \quad \langle g \rangle := \int_{\Omega_v} g(v) \, \mathrm{d}v. \tag{2.13}$$

Recall that we have $\phi(v) = 1$ with $K = 1$ in (2.6) for the linear two-velocity model and $\phi(v) = \left(1, v, \frac{1}{2}|v|^2\right)^\top$ with $K = 3$ in (2.10) for the BGK model.

- Equilibrium: in the stiff limit as $\epsilon \to 0$,

$$\mathcal{Q}(f) = 0 \quad \Leftrightarrow \quad f = M_U[f] = M_U[U] \tag{2.14}$$

where $U = \langle f\phi \rangle$ are the moments of f, and M_U only depends on f through the moments U.

The hyperbolic relaxation system (2.2) and BGK model (2.7) clearly belong to (2.12) with $\mathcal{Q}(f) = M_U - f$.

If we discretize the transport term in (2.12) by a SL scheme, and introduce $\frac{\mathrm{d}}{\mathrm{d}t}$ as the material derivative along characteristics, then we have

$$\frac{\mathrm{d}}{\mathrm{d}t} f \doteq \partial_t f + v \cdot \nabla_x f = \frac{1}{\epsilon}\mathcal{Q}(f). \tag{2.15}$$

From now on, we shall restrict ourselves to the 1D in both space and velocity case and focus on the abstract ODE

$$\frac{\mathrm{d}}{\mathrm{d}t} f = \frac{1}{\epsilon}\mathcal{Q}(f). \tag{2.16}$$

3. New DIRK methods for (2.16). Due to the stiffness in (2.16) when $\epsilon \to 0$ and the consideration of asymptotic preservation property, it is natural for us to choose the DIRK method as the time integration method in the SL scheme, e.g. see the SL nodal discontinuous Galerkin (NDG) scheme [15]. However, when investigating the proposed schemes in the limiting fluid regime, order reduction is sometimes numerically observed. For example, only second order temporal convergence is observed when a classical 3-stage DIRK3 method (B2) is used for integration along characteristics, as shown in Figures 5.3. Such order reduction motivates us to perform accuracy analysis when $\epsilon \ll 1$. In this section, we present accuracy analysis in the fluid regime, as well as the procedure of constructing high order AA DIRK methods, for solving (2.16). To the best of our knowledge, this is the first time that the extra order condition is recognized and truly third order DIRK discretization methods for the limiting fluid regime are constructed in the SL setting.

3.1. The standard DIRK methods. In the scope of our current work, we keep physical and phase space continuous and consider only the DIRK discretization of the collision operator $\mathcal{Q}$ along characteristic lines. Assume a DIRK method with s

stages is characterized by the Butcher tableau $\begin{array}{c|c} \mathbf{c} & \mathrm{A} \\ \hline & \mathbf{b}^T \end{array}$ with invertible $A = (a_{i,j}) \in \mathbb{R}^{s\times s}$, intermediate coefficient vector $\mathbf{c} = [c_1, \cdots c_s]^T$, and quadrature weights $\mathbf{b}^T = [b_1, \cdots b_s]$. For the AP property, we consider only stiffly accurate (SA) DIRK method, i.e. $c_s = 1$ and $A(s,:) = \mathbf{b}^T$ (c.f. [13, Definition 3.2]), so that f^{n+1} coincides with the last stage of the DIRK scheme.

For simplicity of notation, let $f^n = f^n(x,v)$ and $f^{(k)} = f^{(k)}(x,v)$ to be the numerical solution at time t^n and the intermediate numerical solution at $t^{(k)} = t^n + c_k\Delta t$, $k = 1, \cdots s$ respectively. Apply a DIRK method in the above Butcher tableau to (2.16), the internal $f^{(k)}$ is given by,

$$\text{(3.1)}\quad \textbf{The f scheme: } f^{(k)} = f^n + \frac{\Delta t}{\epsilon}\sum_{j=1}^{k-1} a_{kj}\mathcal{Q}(f^{(j)}) + \frac{\Delta t}{\epsilon}a_{kk}\mathcal{Q}(f^{(k)}), \quad k = 1, \cdots s$$

where the time step $\Delta t = t^{n+1} - t^n$. Due to the SA property, $f^{n+1} = f^{(s)}$. Note that, in the f scheme, f^n and $f^{(j)}$ appeared in the k-th equation are evaluated at characteristic feet $(x - c_k v\Delta t, v, t^n)$ and $(x - (c_k - c_j)v\Delta t, v, t^{(j)})$ respectively. On the other hand, when handling the nonlinear relaxation term $\mathcal{Q}(f^{(k)}) = M_U^{(k)} - f^{(k)}$, we first predict the local Maxwellian $M_U^{(k)}$ associated with U^k by taking moments of (3.1) using the conservation property and then compute $f^{(k)}$ via implicit time discretization solvers along the characteristics. For more details, we refer to [15] about how to (1) use the SL NDG scheme for approximating $f^n \approx f(x - c_k v\Delta t, v, t^n)$ and $f^{(j)} \approx f(x - (c_k - c_j)v\Delta t, v, t^{(j)})$; (2) mitigate the nonlinearity in $\mathcal{Q}(f^{(k)})$ with an explicit procedure at each intermediate time stage.

In the following Lemma 3.1, we rewrite (3.1) in the Shu-Osher form [31], which offers convenience for deriving order conditions in the limiting fluid regime.

LEMMA 3.1 (The f scheme in Shu-Osher form). *Assume $a_{kk} > 0$. Then (3.1) is equivalent to*

$$\text{(3.2)}\qquad f^{(k)} = \Big(1 - \sum_{j=1}^{k-1} b_{kj}\Big) f^n + \sum_{j=1}^{k-1} b_{kj} f^{(j)} + \frac{\Delta t}{\epsilon}a_{kk}\mathcal{Q}(f^{(k)}), \quad k = 1, \cdots s$$

where the coefficients b_{kj} are given by the iterative relation

$$\text{(3.3)}\qquad b_{kj} = \frac{a_{kj}}{a_{jj}} - \sum_{l=j+1}^{k-1} \frac{a_{kl}b_{lj}}{a_{ll}}, \quad k > j \geq 1.$$

Proof. We use induction on k. For $k = 1$, both (3.1) and (3.2) gives

$$f^{(1)} = f^n + \frac{\Delta t}{\epsilon} a_{11} \mathcal{Q}(f^{(1)}). \tag{3.4}$$

Assume (3.1) and (3.2) are equivalent for $f^{(j)}$ with $j = 1, \cdots k-1$. Then by solving for $\frac{\Delta t}{\epsilon}\mathcal{Q}(f^{(j)})$ from (3.2) for $f^{(j)}$ we get

$$\frac{\Delta t}{\epsilon}\mathcal{Q}(f^{(j)}) = \frac{1}{a_{jj}}\left(f^{(j)} - \Big(1 - \sum_{l=1}^{j-1} b_{jl}\Big) f^n - \sum_{l=1}^{j-1} b_{jl} f^{(l)} \right). \tag{3.5}$$

Then substitute into (3.1) for $f^{(k)}$ gives

(3.6)

$$\begin{aligned}
f^{(k)} =& f^n + \sum_{j=1}^{k-1} \frac{a_{kj}}{a_{jj}} \Big(f^{(j)} - \Big(1 - \sum_{l=1}^{j-1} b_{jl}\Big) f^n - \sum_{l=1}^{j-1} b_{jl} f^{(l)} \Big) + \frac{\Delta t}{\epsilon} a_{kk} \mathcal{Q}(f^{(k)}) \\
=& \left(1 - \sum_{j=1}^{k-1} \frac{a_{kj}}{a_{jj}} + \sum_{j=1}^{k-1} \frac{a_{kj}}{a_{jj}} \sum_{l=1}^{j-1} b_{jl} \right) f^n + \sum_{j=1}^{k-1} \frac{a_{kj}}{a_{jj}} f^{(j)} - \sum_{j=1}^{k-1} \frac{a_{kj}}{a_{jj}} \sum_{l=1}^{j-1} b_{jl} f^{(l)} + \frac{\Delta t}{\epsilon} a_{kk} \mathcal{Q}(f^{(k)}) \\
=& \left(1 - \sum_{j=1}^{k-1} \frac{a_{kj}}{a_{jj}} + \sum_{l=1}^{k-2} \sum_{j=l+1}^{k-1} \frac{a_{kj}}{a_{jj}} b_{jl} \right) f^n + \sum_{j=1}^{k-1} \frac{a_{kj}}{a_{jj}} f^{(j)} - \sum_{l=1}^{k-2} \sum_{j=l+1}^{k-1} \frac{a_{kj}}{a_{jj}} b_{jl} f^{(l)} + \frac{\Delta t}{\epsilon} a_{kk} \mathcal{Q}(f^{(k)}) \\
=& \left(1 - \sum_{j=1}^{k-1} \frac{a_{kj}}{a_{jj}} + \sum_{j=1}^{k-2} \sum_{l=j+1}^{k-1} \frac{a_{kl}}{a_{ll}} b_{lj} \right) f^n + \sum_{j=1}^{k-1} \frac{a_{kj}}{a_{jj}} f^{(j)} - \sum_{j=1}^{k-2} \sum_{l=j+1}^{k-1} \frac{a_{kl}}{a_{ll}} b_{lj} f^{(j)} + \frac{\Delta t}{\epsilon} a_{kk} \mathcal{Q}(f^{(k)}) \\
=& \Big(1 - \sum_{j=1}^{k-1} b_{kj}\Big) f^n + \sum_{j=1}^{k-1} b_{kj} f^{(j)} + \frac{\Delta t}{\epsilon} a_{kk} \mathcal{Q}(f^{(k)}),
\end{aligned}$$

where we changed summation order in the third equality, and exchange the summation indices j and l in the fourth equality. The result is exactly (3.2). ∎

3.2. Accuracy analysis in the limiting fluid regime. In this section, we derive order conditions of DIRK schemes (up to third order) for the limiting fluid regime in the SL framework. The desired order conditions are obtained by first performing the Taylor expansion of the exact and numerical solutions up to order Δt^4 for both $\epsilon = O(1)$ and ϵ being very small (in particular, $\epsilon \ll \Delta t$); then equating the coefficients of the corresponding high order terms. Uniform accuracy of the SL schemes in the intermediate regime when the spatial mesh size $\Delta x = O(\epsilon)$ are beyond the scope of our current work. We refer to [6, 34] for more derivation details of the order conditions for RK methods.

Hence, assuming the initial data is *well-prepared* (or *consistent*), i.e., $f^0 = M[f^0]$ if $\epsilon \ll 1$,[5] we will show that

(1) The first and second order accuracy of (3.2) in the kinetic regime imply the corresponding accuracy in the fluid regime. See Theorem 3.5.

(2) The third order accuracy of (3.2) in the kinetic regime *does not* imply its third order accuracy in the fluid regime. In fact, assuming its third order accuracy in the kinetic regime, one needs one more order condition to guarantee the third order accuracy in the fluid regime. See Theorem 3.6. In particular, this leads to the order degeneracy of the classical 3-stage DIRK3 method (B2) mentioned previously when the SL NDG method [15] is applied to the BGK equation (2.7) with small ϵ.

3.2.1. The underlying DIRK scheme in the kinetic regime (the f scheme). To analyze the accuracy of the f scheme (3.2), we use $\mathcal{Q}'$ and $\mathcal{Q}''$, the first and second order Fréchet derivatives of $\mathcal{Q}$, defined by

(3.7)
$$\mathcal{Q}'(f)g = \lim_{\delta\to 0}\frac{\mathcal{Q}(f+\delta g)-\mathcal{Q}(f)}{\delta}, \quad \mathcal{Q}''(f)(g_1,g_2) = \lim_{\delta\to 0}\frac{\mathcal{Q}'(f+\delta g_1)g_2-\mathcal{Q}'(f)g_2}{\delta}.$$

There holds the Taylor expansion

$$\mathcal{Q}(f+\delta g) = \mathcal{Q}(f) + \delta\mathcal{Q}'(f)g + \frac{1}{2}\delta^2\mathcal{Q}''(f)(g,g) + O(\delta^3) \tag{3.8}$$

for δ small.

By induction, it is straightforward to show the following Taylor expansion for (3.2), or equivalently, (3.1):

LEMMA 3.2. *The $f^{(k)}$ given by (3.1) satisfies*

$$\begin{aligned} f^{(k)} =& f^n + c_k\frac{\Delta t}{\epsilon}\mathcal{Q}(f^n) + d_k\frac{\Delta t^2}{\epsilon^2}\mathcal{Q}'(f^n)\mathcal{Q}(f^n) \\ &+ \frac{\Delta t^3}{\epsilon^3}\Big(g_k\mathcal{Q}''(f^n)(\mathcal{Q}(f^n),\mathcal{Q}(f^n)) + h_k\mathcal{Q}'(f^n)\mathcal{Q}'(f^n)\mathcal{Q}(f^n)\Big) + O(\frac{\Delta t^4}{\epsilon^4}), \end{aligned} \tag{3.9}$$

where the coefficients c_k, d_k, g_k, h_k satisfy the iterative relations

$$c_k = \sum_{j=1}^{k-1} b_{kj}c_j + a_{kk}, \quad d_k = \sum_{j=1}^{k-1} b_{kj}d_j + a_{kk}c_k, \tag{3.10a}$$

[5] If the initial data is not well-prepared, then (3.1) may reduce to first order. This is similar to the situation of IMEX schemes of type CK. See Theorem 3.6 in [13] and the discussion afterwards.

(3.10b) $$g_k = \sum_{j=1}^{k-1} b_{kj} g_j + \frac{1}{2} a_{kk} c_k^2, \quad h_k = \sum_{j=1}^{k-1} b_{kj} h_j + a_{kk} d_k.$$

Proof. For simplicity we only provide the proof of the iterative relations (3.10a) for c_k and d_k by second order Taylor expansion. The other two relations can be proved similarly by expanding to third order. The fact that $c_k = \sum_{j=1}^{k} a_{kj}$ being the coefficient of the $O(\frac{\Delta t}{\epsilon})$ term for $f^{(k)}$ follows from the Taylor expansion of (3.1). To prove (3.10a), notice that the Taylor expansion of (3.2) up to second order gives

$$\begin{aligned} & f^n + c_k \frac{\Delta t}{\epsilon} \mathcal{Q}(f^n) + d_k \frac{\Delta t^2}{\epsilon^2} \mathcal{Q}'(f^n)\mathcal{Q}(f^n) \\ =& \Big(1 - \sum_{j=1}^{k-1} b_{kj}\Big) f^n + \sum_{j=1}^{k-1} b_{kj} \Big(f^n + c_j \frac{\Delta t}{\epsilon} \mathcal{Q}(f^n) + d_j \frac{\Delta t^2}{\epsilon^2} \mathcal{Q}'(f^n)\mathcal{Q}(f^n) \Big) \\ & + \frac{\Delta t}{\epsilon} a_{kk} \Big(\mathcal{Q}(f^n) + c_k \frac{\Delta t}{\epsilon} \mathcal{Q}'(f^n)\mathcal{Q}(f^n) \Big) + O(\frac{\Delta t^3}{\epsilon^3}), \end{aligned} \tag{3.11}$$

where we used

(3.12)
$$\mathcal{Q}(f^{(k)}) = \mathcal{Q}\Big(f^n + c_k \frac{\Delta t}{\epsilon} \mathcal{Q}(f^n) + O(\frac{\Delta t^2}{\epsilon^2}) \Big) = \mathcal{Q}(f^n) + c_k \frac{\Delta t}{\epsilon} \mathcal{Q}'(f^n)\mathcal{Q}(f^n) + O(\frac{\Delta t^2}{\epsilon^2}).$$

Comparing the $O(\frac{\Delta t}{\epsilon})$ and $O(\frac{\Delta t^2}{\epsilon^2})$ terms gives (3.10a) respectively. ∎

It is straightforward to show that the exact solution to (2.16) satisfies the Taylor expansion

$$\begin{aligned} & f^{n+1} = f^n + \frac{\Delta t}{\epsilon} \mathcal{Q}(f^n) + \frac{1}{2} \frac{\Delta t^2}{\epsilon^2} \mathcal{Q}'(f^n)\mathcal{Q}(f^n) \\ & + \frac{\Delta t^3}{\epsilon^3} \left(\frac{1}{6} \mathcal{Q}''(f^n)(\mathcal{Q}(f^n), \mathcal{Q}(f^n)) + \frac{1}{6} \mathcal{Q}'(f^n)\mathcal{Q}'(f^n)\mathcal{Q}(f^n) \right) + O(\frac{\Delta t^4}{\epsilon^4}). \end{aligned} \tag{3.13}$$

Therefore, comparing (3.9) and (3.13), we have the order conditions for (3.1) in the kinetic regime $\epsilon = O(1)$:

(3.14) $$\text{First order: } c_s = 1, \quad \text{Second order: } d_s = \frac{1}{2}, \quad \text{Third order: } g_s = h_s = \frac{1}{6}.$$

3.2.2. The limiting scheme (the U scheme). In the limiting fluid regime, as $\epsilon \to 0$, f will be relaxed to the equilibrium state $M_U[f]$ for the BGK model. Thus, taking the moments of (2.7) in the fluid regime, we have the limiting fluid equation for U:

(3.15) $$\partial_t U = \mathcal{T}(U), \quad \mathcal{T}(U) := -\partial_x \langle v M_U[U](x,v) \phi(v) \rangle.$$

Therefore, the Taylor expansion of its exact solution is given by

$$
\begin{aligned}
U^{n+1} &= U^n + \Delta t \mathcal{T}(U^n) + \Delta t^2 \frac{1}{2}\mathcal{T}'(U^n)\mathcal{T}(U^n) \\
&+ \Delta t^3 \left(\frac{1}{6}\mathcal{T}''(U^n)\big(\mathcal{T}(U^n), \mathcal{T}(U^n)\big) + \frac{1}{6}\mathcal{T}'(U^n)\mathcal{T}'(U^n)\mathcal{T}(U^n) \right) + O(\Delta t^4),
\end{aligned} \tag{3.16}
$$

which is similar to (3.13).

Taking moments of the f scheme in Shu-Osher form (3.2) against the collision invariants $\phi(v)$ gives

$$
U^{(k)}(x) = (1 - \sum_{j=1}^{k-1} b_{kj})\langle f^n(x - c_k v\Delta t, v)\phi(v)\rangle + \sum_{j=1}^{k-1} b_{kj}\langle f^{(j)}(x - (c_k - c_j)v\Delta t, v)\phi(v)\rangle, \tag{3.17}
$$

where $U^{(k)}(x) := \langle f^{(k)}\phi(v)\rangle$ are the moments of $f^{(k)}$. The collision operator in (3.2) vanishes due to the property that the moments of the relaxation term are identically zero. Meanwhile, as $\epsilon \to 0$, $f^{(k)}$ and f^{n+1} will be relaxed to the local equilibriums $M_U^{(k)}$ and M_U^{n+1} respectively. Thus the limiting scheme for U in (3.15) is given by the following **U scheme**, for $k = 1, \cdots s$,

$$
U^{(k)}(x) = \Big(1 - \sum_{j=1}^{k-1} b_{kj}\Big)\langle M_U[U^n](x - c_k v\Delta t, v)\phi(v)\rangle + \sum_{j=1}^{k-1} b_{kj}\langle M_U[U^{(j)}](x - (c_k - c_j)v\Delta t, v)\phi(v)\rangle. \tag{3.18}
$$

Now we analyze the accuracy of the limiting U scheme (3.18). By Taylor expansion,

$$
\begin{aligned}
\langle M_U[U](x - v\Delta t, v)\phi(v)\rangle =& \langle M_U[U](x, v)\phi(v)\rangle - \Delta t\langle v\partial_x(M_U[U](x, v))\phi(v)\rangle \\
&+ \frac{1}{2}\Delta t^2\langle v^2\partial_{xx}(M_U[U](x, v))\phi(v)\rangle \\
&- \frac{1}{6}\Delta t^3\langle v^3\partial_{xxx}(M_U[U](x, v))\phi(v)\rangle + O(\Delta t^4) \\
=& U + \Delta t\mathcal{T}(U) + \Delta t^2\mathcal{B}(U) + \Delta t^3\tilde{\mathcal{B}}(U) + O(\Delta t^4),
\end{aligned} \tag{3.19}
$$

where

$$
\begin{aligned}
\mathcal{B}(U) &:= \frac{1}{2}\langle v^2\partial_{xx}(M_U[U](x, v))\phi(v)\rangle, \\
\tilde{\mathcal{B}}(U) &:= -\frac{1}{6}\langle v^3\partial_{xxx}(M_U[U](x, v))\phi(v)\rangle,
\end{aligned} \tag{3.20}
$$

are not the same as $\mathcal{T}'\mathcal{T}$, $\mathcal{T}''(\mathcal{T}, \mathcal{T})$ or $\mathcal{T}'\mathcal{T}'\mathcal{T}$.

REMARK 3.3. *In fact, one can write*

$$
\begin{aligned}
\mathcal{T}'(U)\mathcal{T}(U) &= \partial_x\langle v\nabla_U M_U[U](x, v)\phi(v)\cdot\mathcal{T}(U)\rangle, \\
\mathcal{B}(U) &= \partial_x\langle v\nabla_U M_U[U](x, v)\phi(v)\cdot\partial_x(vU)\rangle,
\end{aligned} \tag{3.21}
$$

where $\nabla_U M_U$ means the gradient of the map $U \mapsto M_U[U](v)$ at each x. $\mathcal{T}'(U)\mathcal{T}(U)$ and $\mathcal{B}(U)$ are clearly not the same, since $vU = v\langle M_U[U](v)\phi(v)\rangle \neq \langle vM_U[U](v)\phi(v)\rangle$. One can similarly check that $\tilde{\mathcal{B}}(U)$ is not a linear combination of $\mathcal{T}''(U)(\mathcal{T}(U),\mathcal{T}(U))$ and $\mathcal{T}(U)'\mathcal{T}(U)'\mathcal{T}(U)$.

For the simple model (2.2), one has $2\mathcal{B}(U) = \partial_{xx}U$ and $\mathcal{T}'(U)\mathcal{T}(U) = b^2\partial_{xx}U$. Although they only differ by a constant multiple b^2, one cannot treat them as similar terms if one wants an accurate scheme with coefficients independent of the parameter b in the model. For the third order terms, the situation is similar: one has $6\tilde{\mathcal{B}}(U) = -b\partial_{xxx}U$, $\mathcal{T}'(U)\mathcal{T}'(U)\mathcal{T}(U) = -b^3\partial_{xxx}U$, and $\mathcal{T}''(U)(\mathcal{T}(U),\mathcal{T}(U)) = 0$.

Therefore the limiting scheme (3.18) has the following expression, up to third order accuracy:

(3.22)
$$U^{(k)} = \Big(1 - \sum_{j=1}^{k-1} b_{kj}\Big)\Big(U^n + \Delta t c_k \mathcal{T}(U^n) + \Delta t^2 c_k^2 \mathcal{B}(U^n) + \Delta t^3 c_k^3 \tilde{\mathcal{B}}(U^n)\Big)$$
$$+ \sum_{j=1}^{k-1} b_{kj}\Big(U^{(j)} + \Delta t(c_k - c_j)\mathcal{T}(U^{(j)}) + \Delta t^2(c_k - c_j)^2\mathcal{B}(U^{(j)}) + \Delta t^3(c_k - c_j)^3\tilde{\mathcal{B}}(U^{(j)})\Big) + O(\Delta t^4).$$

This can be viewed as an explicit RK scheme for the limiting equation (written in Shu-Osher form), with some error terms on second and third order. By induction one can show the following Taylor expansion:

LEMMA 3.4. *The $U^{(k)}$ given by (3.22) satisfies*

(3.23)
$$\begin{aligned} U^{(k)} =& U^n + C_k\Delta t\mathcal{T}(U^n) + D_k\Delta t^2\mathcal{T}'(U^n)\mathcal{T}(U^n) + B_k\Delta t^2\mathcal{B}(U^n) \\ &+ \Delta t^3\Big(G_k\mathcal{T}''(U^n)(\mathcal{T}(U^n),\mathcal{T}(U^n)) + H_k\mathcal{T}'(U^n)\mathcal{T}'(U^n)\mathcal{T}(U^n) + B_k^*\mathcal{T}'(U^n)\mathcal{B}(U^n) \\ &+ B_k^{**}\mathcal{B}'(U^n)\mathcal{T}(U^n) + B_k^{***}\tilde{\mathcal{B}}(U^n)\Big) + O(\Delta t^4), \end{aligned}$$

where the coefficients $D_k, B_k, G_k, H_k, B_k^*, B_k^{**}, B_k^{***}$ satisfy the iterative relations

(3.24a)
$$C_k = c_k, \quad D_k = \sum_{j=1}^{k-1} b_{kj}(D_j + (c_k - c_j)c_j),$$

(3.24b)
$$B_k = \Big(1 - \sum_{j=1}^{k-1} b_{kj}\Big)c_k^2 + \sum_{j=1}^{k-1} b_{kj}(B_j + (c_k - c_j)^2),$$

$$G_k = \sum_{j=1}^{k-1} b_{kj}(G_j + \frac{1}{2}(c_k - c_j)c_j^2), \quad H_k = \sum_{j=1}^{k-1} b_{kj}(H_j + (c_k - c_j)D_j), \tag{3.24c}$$

$$B_k^* = \sum_{j=1}^{k-1} b_{kj}(B_j^* + (c_k - c_j)B_j), \quad B_k^{**} = \sum_{j=1}^{k-1} b_{kj}(B_j^{**} + (c_k - c_j)^2 c_j), \tag{3.24d}$$

$$B_k^{***} = \Big(1 - \sum_{j=1}^{k-1} b_{kj}\Big)c_k^3 + \sum_{j=1}^{k-1} b_{kj}(B_j^{***} + (c_k - c_j)^3). \tag{3.24e}$$

This lemma can be proved by using the Taylor expansion of (3.22) up to third order, and we omit the proof since it is similar to the proof of Lemma 3.2.

The order conditions of the U scheme (3.22) are

$$\begin{aligned} &\text{First order: } C_s = 1, \quad \text{Second order: } D_s = \frac{1}{2}, \quad B_s = 0, \\ &\text{Third order: } G_s = H_s = \frac{1}{6}, \quad B_s^* = B_s^{**} = B_s^{***} = 0. \end{aligned} \tag{3.25}$$

3.3. Analysis for first and second order. We analyze the relation between the accuracy of the f scheme and the U scheme by finding relations between their Taylor coefficients. We first consider first and second order accuracy:

THEOREM 3.5. *The first and second order accuracy of the f scheme imply the corresponding accuracy of the U scheme.*

Proof. Since the first order condition for the f scheme and the U scheme are the same ($C_s = c_s$), the first order accuracy of the f scheme implies that of the U scheme.

To show the conclusion for second order accuracy, we will prove the following relations:

$$d_k + D_k = c_k^2, \quad B_k = d_k - D_k. \tag{3.26a}$$

From the second order accuracy of the f scheme, we have $c_s = 1$, $d_s = 1/2$. With (3.26), we obtain $C_s = 1$, $D_s = 1/2$, and then $B_s = 0$, which verifies the order conditions for the second order scheme in (3.25).

We prove (3.26) by induction. For $k = 1$, one has

$$d_1 = a_{11}^2, \quad D_1 = 0, \quad B_1 = c_1^2 = a_{11}^2, \tag{3.27}$$

and thus (3.26) holds for $k = 1$. Suppose the conclusion holds for $j = 1, \cdots k-1$. To show (3.26a), we notice that (by induction hypothesis)

(3.28)
$$D_k = \sum_{j=1}^{k-1} b_{kj}(D_j + (c_k - c_j)c_j) = \sum_{j=1}^{k-1} b_{kj}(c_j^2 - d_j + (c_k - c_j)c_j) = \sum_{j=1}^{k-1} b_{kj}(-d_j + c_k c_j).$$

Summing with the (3.10a) gives

$$d_k + D_k = \sum_{j=1}^{k-1} b_{kj} c_k c_j + a_{kk} c_k = c_k \Big(\sum_{j=1}^{k-1} b_{kj} c_j + a_{kk} \Big) = c_k^2. \tag{3.29}$$

To show (3.26a),

(3.30)
$$\begin{aligned} B_k =& \Big(1 - \sum_{j=1}^{k-1} b_{kj}\Big) c_k^2 + \sum_{j=1}^{k-1} b_{kj}(B_j + (c_k - c_j)^2) = c_k^2 + \sum_{j=1}^{k-1} b_{kj}(d_j - D_j - 2c_k c_j + c_j^2) \\ =& c_k^2 + \sum_{j=1}^{k-1} b_{kj}(2d_j - 2c_k c_j) = c_k^2 - 2\sum_{j=1}^{k-1} b_{kj}(-d_j + c_k c_j) = c_k^2 - 2D_k = d_k - D_k, \end{aligned}$$

where we started from (3.24b), and then used the induction hypothesis, and finally used (3.28) and (3.26a). ∎

3.4. Analysis for third order.

THEOREM 3.6. *The third order accuracy of the f scheme, together with the condition $G_s = 1/6$, implies the third order accuracy of the U scheme.*

Proof. We will prove the following relations

$$2G_k - H_k + 2g_k = c_k d_k, \tag{3.31a}$$

$$B_k^* = 2G_k - 2H_k, \quad B_k^{**} = 2g_k - 2H_k - c_k^3 + 2c_k D_k, \tag{3.31b}$$

$$B_k^{***} = c_k^3 - 3B_k^{**} - 6G_k. \tag{3.31c}$$

(3.31) implies the conclusion of the theorem. In fact, the third order accuracy of the f scheme gives $c_s = 1$, $d_s = 1/2$, $g_s = h_s = 1/6$. If $G_s = 1/6$, then (3.31a) gives $H_s = 1/6$, and similarly the other three equations of (3.31) give $B_s^* = B_s^{**} = B_s^{***} = 0$ (where we need to use $D_s = 1/2$ by Theorem 3.5).

To prove (3.31a), we define $L_k = 2G_k - H_k$. Then from (3.24c) and (3.26a),

$$L_k = \sum_{j=1}^{k-1} b_{kj}(L_j + (c_k - c_j)d_j). \tag{3.32}$$

We prove by induction that

$$L_k = c_k d_k - 2g_k, \tag{3.33}$$

which is exactly (3.31a). For $k = 1$, $L_1 = 0$, $c_1 d_1 - 2g_1 = a_{11} \cdot a_{11}^2 - 2 \cdot (a_{11}^3/2) = 0$. Suppose the conclusion holds for $j = 1, \cdots k-1$, then

$$\begin{aligned} L_k =& \sum_{j=1}^{k-1} b_{kj}(L_j + (c_k - c_j)d_j) = \sum_{j=1}^{k-1} b_{kj}(c_j d_j - 2g_j + (c_k - c_j)d_j) \\ =& c_k \sum_{j=1}^{k-1} b_{kj} d_j - 2\sum_{j=1}^{k-1} b_{kj} g_j = c_k(d_k - a_{kk}c_k) - 2\sum_{j=1}^{k-1} b_{kj} g_j \\ =& c_k d_k - 2\left(\sum_{j=1}^{k-1} b_{kj} g_j + \frac{1}{2} a_{kk} c_k^2\right) = c_k d_k - 2g_k, \end{aligned} \tag{3.34}$$

where we used the induction hypothesis, (3.10a) and (3.10b). (3.31b) is clear from the (3.24c) and (3.26). Now we show the second equality in (3.31b) by induction. For $k = 1$, $B_1^{**} = 0$, $2g_1 - 2H_1 - c_1^3 - 2c_1 D_1 = 2 \cdot \frac{1}{2} a_{11} c_1^2 - c_1^3 = 0$. Suppose the conclusion

holds for $j = 1, \dots, k-1$, then

(3.35)

$$
\begin{aligned}
B_k^{**} &= \sum_{j=1}^{k-1} b_{kj}(B_j^{**} + (c_k - c_j)^2 c_j) \\
&= \sum_{j=1}^{k-1} b_{kj}(2g_j - 2H_j + 2c_j D_j + c_k^2 c_j - 2c_k c_j^2) \\
&= 2\sum_{j=1}^{k-1} b_{kj} g_j - 2\sum_{j=1}^{k-1} b_{kj} H_j + \sum_{j=1}^{k-1} b_{kj}(2c_j D_j + c_k^2 c_j - 2c_k c_j^2) \\
&= 2(g_k - \frac{1}{2} a_{kk} c_k^2) - 2\Big(H_k - \sum_{j=1}^{k-1} b_{kj}(c_k - c_j) D_j\Big) + \sum_{j=1}^{k-1} b_{kj}(2c_j D_j + c_k^2 c_j - 2c_k c_j^2) \\
&= 2g_k - a_{kk} c_k^2 - 2H_k + \sum_{j=1}^{k-1} b_{kj}(2(c_k - c_j) D_j + 2c_j D_j + c_k^2 c_j - 2c_k c_j^2) \\
&= 2g_k - a_{kk} c_k^2 - 2H_k + c_k \sum_{j=1}^{k-1} b_{kj}(c_k c_j - 2d_j) \\
&= 2g_k - 2H_k - c_k\Big(\sum_{j=1}^{k-1} b_{kj} d_j + a_{kk} c_k\Big) + c_k \sum_{j=1}^{k-1} b_{kj}(c_k c_j - d_j) \\
&= 2g_k - 2H_k - c_k d_k + c_k D_k \\
&= 2g_k - 2H_k - c_k^3 + 2c_k D_k,
\end{aligned}
$$

where we used the induction hypothesis, (3.10b), (3.24c), (3.10a) and (3.28).

To prove (3.31c), notice that

(3.36)

$$
B_k^{***} - c_k^3 = \sum_{j=1}^{k-1} b_{kj}((B_j^{***} - c_j^3) - 3c_k^2 c_j + 3c_k c_j^2) = \sum_{j=1}^{k-1} b_{kj}((B_j^{***} - c_j^3) - 3(c_k - c_j)^2 c_j - 6\cdot\frac{1}{2}(c_k - c_j) c_j^2).
$$

Therefore (3.31c) follows from (3.24d) and (3.24c). ∎

This forms sharp contrast with that of the mesh-based Eulerian IMEX schemes for stiff kinetic equations. It was shown in Theorem 3.3 in [13] that an IMEX of type A (i.e., the implicit table is DIRK) applied to a stiff kinetic equation gives rise to an explicit RK scheme in the fluid regime, whose Butcher table is the same as the explicit table of the IMEX scheme. As a consequence, the k-th order accuracy of such an IMEX scheme in the kinetic regime implies that in the fluid regime, for any $k \geq 1$.

Based on the order conditions in Theorem 3.6, we propose 4-stage DIRK3 methods (B3)-(B10) in Appendix B for both regimes up to third order.

REMARK 3.7. *The classical 3-stage DIRK3 method* (B2) *[7] in the Appendix B does not satisfies the condition* $G_3 = 1/6$ *appeared in Theorem 3.6. In fact, calculation shows that* $G_3 \approx 0.066745$*, and therefore the corresponding U scheme is not third order. This example shows that the condition* $G_s = 1/6$ *is not a consequence of the third order accuracy of the f scheme.*

REMARK 3.8. *There are a lot of freedoms when creating 4-stage DIRK3 methods satisfying Theorem 3.6. For the consideration of computational cost, one could let certain elements of the Butcher tableaus be zeros. For instance, in Table B7 - Table B10, we have two zero elements of* a_{ij}.

4. Stability analysis for DIRK methods. In this section, we analyze the stability property of DIRK schemes under the SL setting. In particular, we are interested in the L-stable DIRK methods for the AP property in the limiting $\epsilon \to 0$ regime. Linear stability of DIRK schemes with different ϵ are investigated. Similar to the accuracy analysis in Section 3, we keep the phase space continuous and consider the linear kinetic problem (2.2) with periodic boundary condition, written in the following form

$$\begin{pmatrix} f_1 \\ f_2 \end{pmatrix}_t + \begin{pmatrix} 1 & 0 \\ 0 & -1 \end{pmatrix} \begin{pmatrix} f_1 \\ f_2 \end{pmatrix}_x = \frac{1}{\epsilon} \begin{pmatrix} M_1 - f_1 \\ M_2 - f_2 \end{pmatrix} \tag{4.1}$$

where $M_U = (M_1, M_2)^T$ satisfies (2.5). In the analysis, we apply DIRK methods in the SL framework to (4.1) and study f_1 and f_2 in the form of Fourier series

$$f_1 = \sum_k \widehat{f}_1^{(k)}(t) e^{ikx} \quad \text{and} \quad f_2 = \sum_k \widehat{f}_2^{(k)}(t) e^{ikx}, \quad i = \sqrt{-1} \tag{4.2}$$

with k is the wavenumber.

Before discussing the stability of general DIRK methods, we first work with the backward Euler method to illustrate the process. Applying the backward Euler to (4.1) along characteristics, gives us

$$\begin{aligned} f_1^{n+1} &= f_1^n(x - \Delta t) + \frac{\Delta t}{\epsilon}(M_1^{n+1} - f_1^{n+1}), \\ f_2^{n+1} &= f_2^n(x + \Delta t) + \frac{\Delta t}{\epsilon}(M_2^{n+1} - f_2^{n+1}). \end{aligned} \tag{4.3}$$

Plugging (4.2) into (4.3), one can obtain the following the relation between the k-th

Fourier modes e^{ikx} at t^{n+1} and t^n:

(4.4)
$$\begin{pmatrix} \widehat{f}_1^{(k)}(t^{n+1}) \\ \widehat{f}_2^{(k)}(t^{n+1}) \end{pmatrix} = \left[I - \frac{\Delta t}{2\epsilon} \begin{pmatrix} -1+b & 1+b \\ 1-b & -1-b \end{pmatrix} \right]^{-1} \begin{pmatrix} e^{-ik\Delta t} & 0 \\ 0 & e^{ik\Delta t} \end{pmatrix} \begin{pmatrix} \widehat{f}_1^{(k)}(t^n) \\ \widehat{f}_2^{(k)}(t^n) \end{pmatrix}$$

with the amplification matrix

$$\begin{aligned} M_{\text{BE}} =& \left[I - \frac{\Delta t}{2\epsilon} \begin{pmatrix} -1+b & 1+b \\ 1-b & -1-b \end{pmatrix} \right]^{-1} \begin{pmatrix} e^{-ik\Delta t} & 0 \\ 0 & e^{ik\Delta t} \end{pmatrix} \\ =& \frac{1}{1+\xi} \begin{pmatrix} 1+\frac{1+b}{2}\xi & \frac{1+b}{2}\xi \\ \frac{1-b}{2}\xi & 1+\frac{1-b}{2}\xi \end{pmatrix} \begin{pmatrix} e^{-ik\Delta t} & 0 \\ 0 & e^{ik\Delta t} \end{pmatrix} \end{aligned} \tag{4.5}$$

where $\xi = \frac{\Delta t}{\epsilon}$. Below we will use $\frac{\Delta t}{\epsilon}$ and ξ interchangeably. Taking the 2-norm of M_{BE}, we have

$$\|M_{\text{BE}}\|_2 \le \left\| \frac{1}{1+\xi} \begin{pmatrix} 1+\frac{1+b}{2}\xi & \frac{1+b}{2}\xi \\ \frac{1-b}{2}\xi & 1+\frac{1-b}{2}\xi \end{pmatrix} \right\|_2 \left\| \begin{pmatrix} e^{-ik\Delta t} & 0 \\ 0 & e^{ik\Delta t} \end{pmatrix} \right\|_2 = 1.$$

In fact, the backward Euler method is unconditionally stable in this context.

Next, we generalize the above analysis to a 2-stage DIRK2 method, e.g. with Butcher tableau (B1). At the first stage $t^{(1)} = t^n + c_1\Delta t$, repeating similar procedure as from (4.3) and (4.4), one can show the Fourier modes at $t^{(1)}$ and t^n are related via

$$\begin{aligned} \begin{pmatrix} \widehat{f}_1^{(k)}(t^{(1)}) \\ \widehat{f}_2^{(k)}(t^{(1)}) \end{pmatrix} =& \frac{1}{1+a_{11}\xi} \begin{pmatrix} 1+\frac{1+b}{2}a_{11}\xi & \frac{1+b}{2}a_{11}\xi \\ \frac{1-b}{2}a_{11}\xi & 1+\frac{1-b}{2}a_{11}\xi \end{pmatrix} \begin{pmatrix} e^{-ikc_1\Delta t} & 0 \\ 0 & e^{ikc_1\Delta t} \end{pmatrix} \begin{pmatrix} \widehat{f}_1^{(k)}(t^n) \\ \widehat{f}_2^{(k)}(t^n) \end{pmatrix} \\ \doteq& M_{\text{DIRK2, (1)}} \begin{pmatrix} \widehat{f}_1^{(k)}(t^n) \\ \widehat{f}_2^{(k)}(t^n) \end{pmatrix} \end{aligned} \tag{4.6}$$

with amplification matrix $M_{\text{DIRK2, (1)}}$. At the second (i.e. final) stage t^{n+1}, using (3.2), we have the following formulation in the Shu-Osher form

$$\begin{aligned} f_1^{n+1} &= (1-b_{21})f_1^n(x-\Delta t) + b_{21}f_1^{(1)}(x-(1-c_1)\Delta t) + \frac{a_{22}\Delta t}{\epsilon}(M_1^{n+1} - f_1^{n+1}), \\ f_2^{n+1} &= (1-b_{21})f_2^n(x+\Delta t) + b_{21}f_2^{(1)}(x+(1-c_1)\Delta t) + \frac{a_{22}\Delta t}{\epsilon}(M_2^{n+1} - f_2^{n+1}). \end{aligned} \tag{4.7}$$

For the notation simplicity, for $l = 2, \cdots s,\ l > j \geq 1$, we introduce

$$A_l = I - \frac{a_{ll}\Delta t}{\epsilon}\begin{pmatrix} \frac{-1+b}{2} & \frac{1+b}{2} \\ \frac{1-b}{2} & \frac{-1-b}{2} \end{pmatrix}, \quad B_l = (1 - \sum_{j=1}^{l-1} b_{lj}) \begin{pmatrix} e^{-ikc_l\Delta t} & 0 \\ 0 & e^{ikc_l\Delta t} \end{pmatrix} \tag{4.8}$$

$$C_{lj} = b_{lj} \begin{pmatrix} e^{-ik(c_l - c_j)\Delta t} & 0 \\ 0 & e^{ik(c_l - c_j)\Delta t} \end{pmatrix}$$

for the operations involving intermediate stage values at $t^{(j)}, j = 1, \cdots l$. With notations in (4.8), (4.7) leads to

$$\begin{pmatrix} \widehat{f}_1^{(k)}(t^{n+1}) \\ \widehat{f}_2^{(k)}(t^{n+1}) \end{pmatrix} = A_2^{-1}\left[B_2 \begin{pmatrix} \widehat{f}_1^{(k)}(t^{n}) \\ \widehat{f}_2^{(k)}(t^{n}) \end{pmatrix} + C_{21} \begin{pmatrix} \widehat{f}_1^{(k)}(t^{(1)}) \\ \widehat{f}_2^{(k)}(t^{(1)}) \end{pmatrix} \right] \tag{4.9}$$

Combining (4.6) and (4.9), we have

(4.10)

$$\begin{pmatrix} \widehat{f}_1^{(k)}(t^{n+1}) \\ \widehat{f}_2^{(k)}(t^{n+1}) \end{pmatrix} = A_2^{-1}\left[B_2 + C_{21} M_{\text{DIRK2, (1)}}\right] \begin{pmatrix} \widehat{f}_1^{(k)}(t^{n}) \\ \widehat{f}_2^{(k)}(t^{n}) \end{pmatrix} \doteq M_{\text{DIRK2}} \begin{pmatrix} \widehat{f}_1^{(k)}(t^{n}) \\ \widehat{f}_2^{(k)}(t^{n}) \end{pmatrix}.$$

When $\xi \to \infty$, the amplification matrix M_{DIRK2} goes to

(4.11)

$$\begin{pmatrix} \frac{1+b}{2}\left[(1 + \frac{-1+b}{2}b_{21})e^{-ikc_2\Delta t} + \frac{1-b}{2}b_{21}e^{ik(c_2-2c_1)\Delta t}\right] & \frac{1+b}{2}\left[\frac{1+b}{2}b_{21}e^{-ik(c_2-2c_1)\Delta t} + (1 + \frac{-1-b}{2}b_{21})e^{ikc_2\Delta t}\right] \\ \frac{1-b}{2}\left[(1 + \frac{-1+b}{2}b_{21})e^{-ikc_2\Delta t} + \frac{1-b}{2}b_{21}e^{ik(c_2-2c_1)\Delta t}\right] & \frac{1-b}{2}\left[\frac{1+b}{2}b_{21}e^{-ik(c_2-2c_1)\Delta t} + (1 + \frac{-1-b}{2}b_{21})e^{ikc_2\Delta t}\right] \end{pmatrix}$$

and the corresponding eigenvalues are $\lambda_1 = 0$ and

$$\lambda_2 = \left(1 - \frac{1-b^2}{2}b_{21}\right)\cos(kc_2\Delta t) + \frac{1-b^2}{2}b_{21}\cos(k(c_2 - 2c_1)\Delta t).$$

In Figure 4.1, we present the contour plot of $|\lambda_2|$ versus $b \in [0, 1]$ and $k\Delta t \in [0, 2\pi]$, as $\xi = \frac{\Delta t}{\epsilon} \to \infty$. The contour plot of $|\lambda_2|$ in Figure 4.1 is plotted subject to the calculation error of Matlab. We observe that for different $b \in [0, 1]$, different constraints on $k\Delta t$ need to be imposed for stability. For example, one needs to use $k\Delta t \in [0, 1.7927\pi]$ so that $|\lambda_2| \leq 1$ when $b = 0$, while $k\Delta t \in [0, 2\pi]$ is allowed for a bigger b, such as $b = 0.6$ in Example 5.1. In Figure 4.1, we show the contour plot of two eigenvalues for M_{DIRK2} when $b = 0.6$. We consider the range of $k\Delta t \in [0, 2\pi]$ and $\xi \in [0, 10]$. Notice that for ξ greater than 10 and in the limit of ∞, the spectral radius of M_{DIRK2} has been numerically checked to be bounded by 1 with $b = 0.6, k\Delta t \in [0, 2\pi]$. We

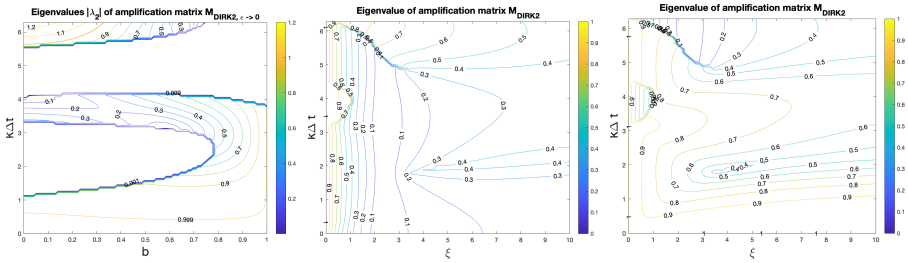

FIG. 4.1. *DIRK2 method in Table B1. Left: contour plot of spectral radius of* $M_{DIRK2,\xi\to\infty}$ *versus* $b \in [0,1]$ *and* $k\Delta t \in [0, 2\pi]$. *Middle and right: contour plot of the eigenvalues* $|\lambda_{1,2}|$ *with* $k\Delta t \in [0, 2\pi]$ *and* $\xi = \frac{\Delta t}{\epsilon} \in [0, 10]$ *for the amplification matrix* M_{DIRK2} *with* $b = 0.6$ *in (4.1). Note that we choose the range of* $\xi \in [0, 10]$ *as an example. It is numerically verified that both eigenvalues are bounded from above by* 1 *for* $\xi > 10$.

note that, the constraint for the range of $k\Delta t$ gives a guidance to the time stepping size one can take, since k is the wave number related to the spatial resolution ranging from 0 to $\frac{\pi}{\Delta x}$, thus the upper bound on $k\Delta t$ provides a time stepping constraint on the CFL $\propto \frac{\Delta t}{\Delta x}$. However, it does not provide a sufficient condition for linear stability, since the spatial operations are kept continuous in the current analysis. Analysis for a fully discrete scheme will be rather involved and out of the scope of current work, especially when feet of characteristics could be located more than one cell away for CFL larger than 1.

Finally, when we perform the linear stability analysis to the proposed 4-stage DIRK3 time discretization methods specified in Butcher Tables B3-B10 for (4.1), the Fourier modes of e^{ikx} for f_1 and f_2 follow the following recursive relation, $l = 2, 3, 4$,

$$\begin{pmatrix} \widehat{f}_1^{(k)}(t^{(l)}) \\ \widehat{f}_2^{(k)}(t^{(l)}) \end{pmatrix} = A_l^{-1} \left[B_l \begin{pmatrix} \widehat{f}_1^{(k)}(t^n) \\ \widehat{f}_2^{(k)}(t^n) \end{pmatrix} + \sum_{j=1}^{l-1} C_{lj} \begin{pmatrix} \widehat{f}_1^{(k)}(t^{(j)}) \\ \widehat{f}_2^{(k)}(t^{(j)}) \end{pmatrix} \right], \tag{4.12}$$

and that

$$\begin{aligned} \begin{pmatrix} \widehat{f}_1^{(k)}(t^{n+1}) \\ \widehat{f}_2^{(k)}(t^{n+1}) \end{pmatrix} &= A_4^{-1} \left[B_4 + \sum_{j=1}^{3} C_{4j} A_j^{-1} E_j \right] \begin{pmatrix} \widehat{f}_1^{(k)}(t^n) \\ \widehat{f}_2^{(k)}(t^n) \end{pmatrix} \\ &= M_{\text{DIRK3}} \begin{pmatrix} \widehat{f}_1^{(k)}(t^n) \\ \widehat{f}_2^{(k)}(t^n) \end{pmatrix} \end{aligned} \tag{4.13}$$

where $E_j = B_j + \sum_{l=1}^{j-1} C_{jl} A_l^{-1} E_l$. We compute the spectral radius of $M_{\text{DIRK3},\epsilon\to 0}$ by Matlab, for which the contour plot is presented in Figure 4.2 with $b \in [0, 1]$ and

$k\Delta t \in [0, 2\pi]$ for DIRK3 methods given in Table B2 - B10. It can be observed that the appropriate ranges of $k\Delta t$ such that $|\lambda_2| \leq 1$ depend on the choice of $b \in [0, 1]$. In particular, when $b = 0.6$, we see that in Figure 4.2(i), with $k\Delta t \in [0, 5]$ which is a considerable wide range for the $k\Delta t$, we have $|\lambda_2| \leq 1$. Compared with other contour plots of λ_2 in Figure 4.2, we found the 4-stage DIRK3 method (B10) being a robust choice for linear stability, as well as asymptotic third order accuracy. Following this observation, in Figure 4.3, we plot the contour plot of $|\lambda_{1,2}|$ for the corresponding amplification matrix M_{DIRK3} when $b = 0.6$ and use $k\Delta t \in [0, 1.5924\pi], \xi \in [0, 10]$. We observe the $|\lambda_{1,2}| \leq 1$ with our choice of ξ and $k\Delta t$ which indicates that when $b = 0.6$ in (4.1), the spectral radius of DIRK3 method (B10) is bounded by 1 for $k\Delta t \in [0, 1.5924\pi]$. Such statement is checked to be valid for all ξ, although only $\xi \in [0, 10]$ is being plotted. For the numerical tests in the next section, we choose the DIRK3 method specified in Table B10 with third order classical accuracy as well as asymptotic accuracy. We also note that the spectral radius of $M_{\text{DIRK3},\epsilon\to 0}$ is slightly larger than 1 toward the lower right corner of the plot in Figure 4.2(i), yet no numerical instability is observed in our tests. It is our future work to optimize DIRK3 methods, that satisfy the extra order condition for asymptotic third order temporal convergence, in terms of their linear stability properties.

5. Numerical Tests. In this section, we apply the SL NDG-DIRK methods proposed in [15] to test the classical and asymptotic temporal orders of convergence for proposed DIRK methods via stiff linear/nonlinear hyperbolic relaxation systems and the kinetic BGK model. Unless otherwise noted, we use a third order SL NDG spatial discretization with a well-resolved mesh of 640 uniformly spaced elements, to minimize the spatial error, and periodic boundary conditions are used for all tests. We also use the time stepping size as $\Delta t = \text{CFL} \cdot \frac{\Delta x}{a}$ where a is the maximum transport speed, and CFL values are to be specified for each test.

EXAMPLE 5.1. *[19] Consider the linear two-velocity model* (2.2) *with* $b = 0.6$ *on* $x \in [0, 1]$, *and the initial condition given by*

$$u(x, 0) = \exp(\sin 2\pi x), \quad v(x, 0) = b \exp(\sin 2\pi x).$$

We test the temporal convergences of different DIRK methods, by plotting in Figure 5.1(a)-

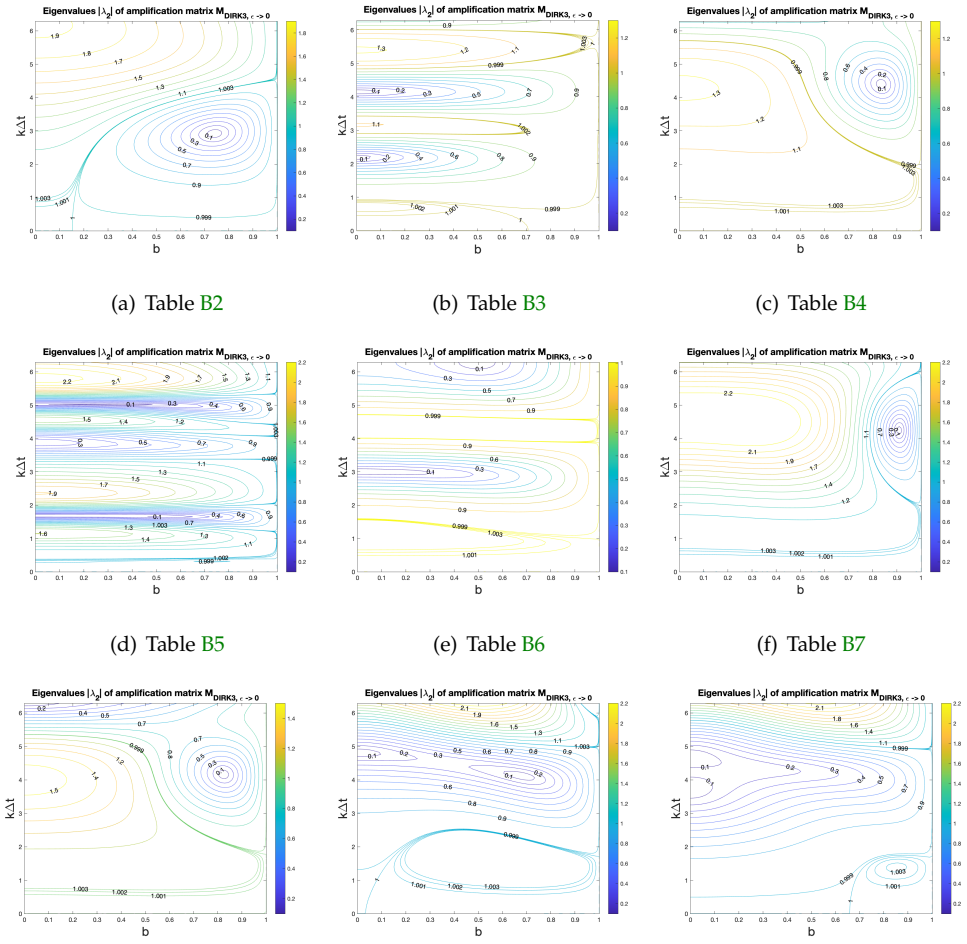

(a) Table B2 (b) Table B3 (c) Table B4

(d) Table B5 (e) Table B6 (f) Table B7

(g) Table B8 (h) Table B9 (i) Table B10

FIG. 4.2. *Contour plot of the eigenvalues* $|\lambda_2|$ *for* $M_{DIRK3,\epsilon\to 0}$ *versus* $b \in [0,1]$ *and* $k\Delta t \in [0, 2\pi]$ *for the DIRK3 method in Table B2 - B10 as* $\xi = \frac{\Delta t}{\epsilon} \to \infty$.

5.1(c) L^1 *errors versus the CFL numbers in* $\epsilon = 10^{-2}, 10^{-5}$ *and* 10^{-6} *regimes at* $T = 0.2$. *In the figures, for backward Euler and DIRK2 methods, we can clearly observe the expected orders of convergence in all three regimes with CFL values as large as* 16; *we also see that the errors stagnates due to dominancy of the spatial errors when CFL* < 0.02 *for the DIRK2 method. Here, we note that, compared with the Eulerian methods, the temporal errors of SL methods computed using reference solutions still depend on* Δx *on a fixed mesh due to the characteristic tracing feature. For the classical 3-stage DIRK3 scheme (B2), we have the following observation: when* $\epsilon = 10^{-2}$, *third order accuracy is observed when*

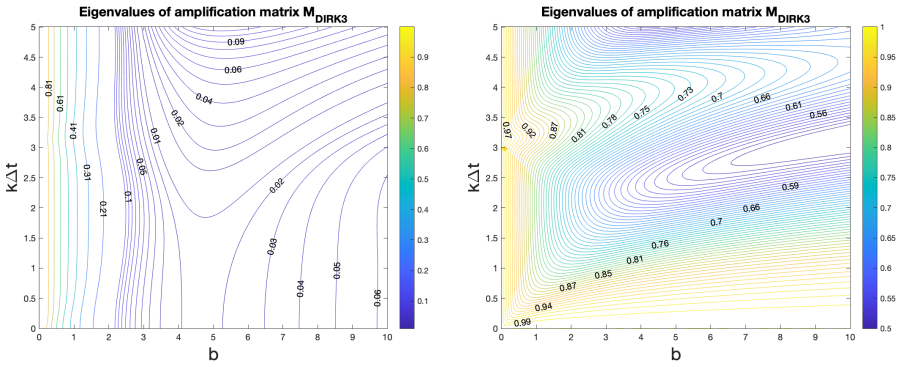

(a) $|\lambda_1|$ (b) $|\lambda_2|$

FIG. 4.3. *Contour plot of the eigenvalues* $|\lambda_{1,2}|$ *with* $k\Delta t \in [0, 1.5924\pi]$ *and* $\xi = \frac{\Delta t}{\epsilon} \in [0, 10]$ *for the amplification matrix* M_{DIRK3} *of the* 4*-stage DIRK3 method in Table B10.* $b = 0.6$ *in* (4.1)*. Note that we choose the range of* $\xi \in [0, 10]$ *as an example, we checked that for* $\xi > 10$*, the eigenvalues are bounded by* 1 *as well.*

CFL > 0.2*; while for* $\epsilon = 10^{-5}$ *and* 10^{-6}*, when* $0.02 <$ *CFL* < 1 *and CFL* > 3*, only second order temporal convergence is observed as shown in Theorem 3.6 together with the Remark 3.7, but the method suffers from the numerical instability when* $1 <$ *CFL* < 3*. Such instability, may be due to the shift of characteristics feet across one computational cell from DG spatial discretization, is not covered in our current analysis. For the 4-stage DIRK3 method (B10), when* $\epsilon = 10^{-2}$*, the expected third order convergence is observed when CFL* > 0.4*; for* $\epsilon = 10^{-5}$ *and* $\epsilon = 10^{-6}$*, the following observations are made with the decrease of the CFL values: when CFL is sufficiently large, the method shows the third order asymptotic accuracy (phase 1), as CFL getting smaller, numerical instability again shows up for CFL* > 1 *(phase 2), then the method continues to converge when CFL is even smaller (phase 3), and eventually the numerical errors are trapped in a plateau with the dominant spatial errors (phase 4). Additionally, we see that the convergence behavior in phase 3 is related to the* ϵ *value: when* $\epsilon = 10^{-5}$*, both third and first order accuracies are observed for* $0.04 <$ *CFL* < 0.1 *(kinetic regime) and* $0.1 <$ *CFL* < 1 *(intermediate regime) respectively; when* $\epsilon = 10^{-6}$*, the convergence reduces to first order accuracy for* $0.1 <$ *CFL* < 1 *(intermediate regime). The accuracy analysis performed in Section 3 considers* $\Delta t \ll \epsilon$ *in the kinetic regime and* $\epsilon \ll \Delta t$ *in the fluid regime. The convergence studies of time discretization methods in intermediate regime, when* ϵ *and* Δt *are on a comparable scale, is not covered in our current analysis.*

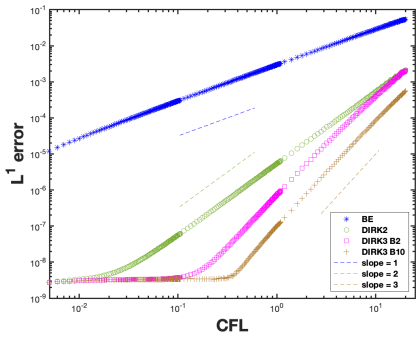

(a) $\epsilon = 10^{-2}$

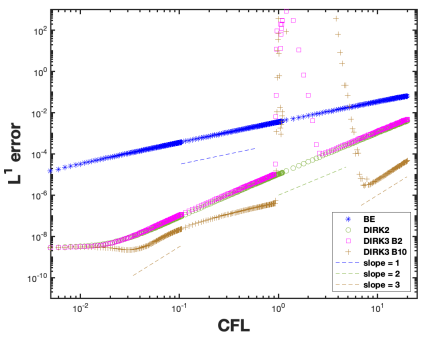

(b) $\epsilon = 10^{-5}$

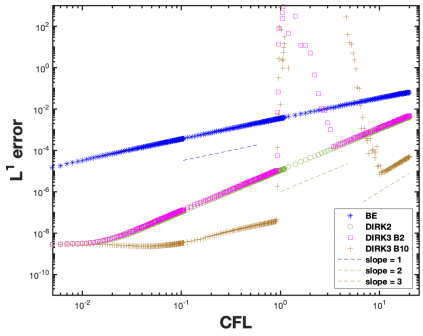

(c) $\epsilon = 10^{-6}$

FIG. 5.1. *Plots of L^1 errors versus CFL of SL NDG-DIRK methods for (2.2) with $b = 0.6$ at $T = 0.2$. The reference solutions are obtained from the corresponding numerical solutions with CFL $= 0.001$. 5.1(a) - 5.1(c): L^1 errors computed on fixed mesh $N_x = 640$ in $\epsilon = 10^{-2}, 10^{-5}, 10^{-6}$ regimes. BE, DIRK2, DIRK3 B2, DIRK3 B10 refer to backward Euler, DIRK2 method (B1), classical 3-stage DIRK3 method (B2) and 4-stage DIRK3 method (B10) respectively. Line segments of slope 1, 2 and 3 are also provided as references.*

EXAMPLE 5.2. *Consider the nonlinear hyperbolic relaxation system in [19],*

$$\begin{cases} \partial_t u + \partial_x v = 0, \\ \partial_t v + \partial_x u = \frac{1}{\epsilon}(bu^2 - v), \end{cases} \tag{5.1}$$

with $b = 0.2$ on $x \in [0, 1]$. When $\epsilon \to 0$, the limit of (5.1) is the Burger's equation $\partial_t u + b\partial_x(u^2) = 0$. Let $f = (f_1, f_2)^T$ where $f_1 = \frac{u+v}{2}, f_2 = \frac{u-v}{2}$, then (5.1) can be reformulated into the two-discrete velocity model:

$$\partial_t f + v\partial_x f = \frac{1}{\epsilon}(M_U - f) \tag{5.2}$$

with $v \in \Omega_v = \{-1, 1\}$ and the local equilibrium $M_U = (\frac{bu^2+u}{2}, \frac{-bu^2+u}{2})^T$. (5.1) has only

one collision invariant $\phi(v) = 1$. *The initial condition for* u *and* v *are given by* $u(x,0) = \frac{1}{2}\exp(\sin 2\pi x)$, $v(x,0) = bu^2(x,0)$. *The final simulation time* $T = 0.2$. *In Figure 5.2, we plot* L^1 *errors versus the CFL numbers for both* $\epsilon = 10^{-2}$ *and* 10^{-6}. *Similar observation as Example 5.1 can be made. When* $\epsilon = 10^{-2}$, *classical orders of convergence are observed for various DIRK schemes with CFL as large as* 16. *When* $\epsilon = 10^{-6}$, *only second order convergence is observed for the classical 3-stage DIRK3 (B2) when* $0.02 < CFL < 0.8$ *and* $CFL > 4$. *Numerical instability again shows up when* $0.8 < CFL < 4$, *which is not covered in our current analysis. We also observe four phases for the 4-stage DIRK3 (B10): third order asymptotic accuracy for* $CFL > 8$ *(phase 1), numerical instability for* $1 < CFL < 8$ *(phase 2), first order accuracy for* $0.03 < CFL < 1$ *(phase 3) and stagnant errors for* $CFL < 0.03$ *(phase 4).*

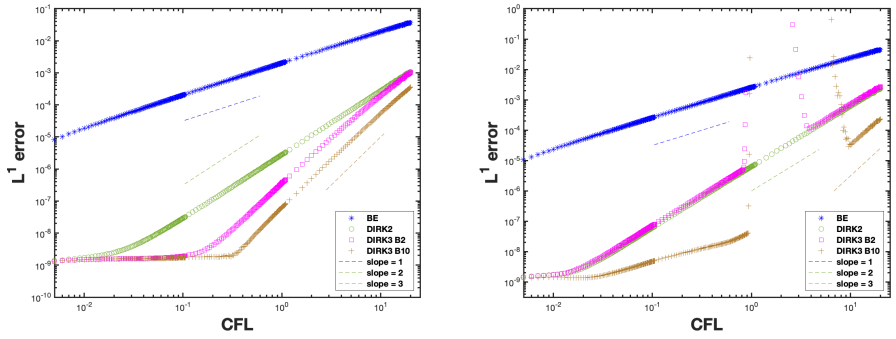

(a) $\epsilon = 10^{-2}$ (b) $\epsilon = 10^{-6}$

FIG. 5.2. *Plots of* L^1 *errors versus CFL on fixed mesh* $N_x = 640$ *for (5.2) in* $\epsilon = 10^{-2}, 10^{-6}$ *regimes at* $T = 0.2$. *The reference solutions are obtained from the corresponding numerical solutions with* $CFL = 0.001$. *BE, DIRK2, DIRK3 B2, DIRK3 B10 refer to backward Euler, DIRK2 method (B1), classical 3-stage DIRK3 method (B2) and 4-stage DIRK3 method (B10) respectively. Line segments of slope 1, 2 and 3 are also provided as references.*

EXAMPLE 5.3. *Consider 1D1V BGK equation (2.7) with the consistent initial distribution in [29]*

$$f(x,v,0) = \frac{\rho_0}{\sqrt{2\pi T_0}} \exp\left(-\frac{(v-u_0(x))^2}{2T_0}\right), \quad x \in [-1,1] \tag{5.3}$$

and initial velocity

$$u_0 = \frac{1}{10}\left[\exp\left(-(10x-1)^2\right) - 2\exp\left(-(10x+3)^2\right)\right]. \tag{5.4}$$

Initial density and temperature are uniform with constant values $\rho(x,0) = \rho_0 = 1$ *and* $T(x,0) = T_0 = 1$ *respectively. The test is performed on the velocity domain* $v \in [-15, 15]$*, which is uniformly discretized with* $N_v = 100$ *grid points. The temporal accuracies of the SL NDG-DIRK method [15] when applied to* (5.3) *with* $\epsilon = 10^{-2}$ *and* 10^{-6} *at* $T = 0.04$ *are given in Figure 5.3. As the previous examples, classical orders of convergence are observed for* $\epsilon = 10^{-2}$ *with large CFL numbers. But both the classical 3-stage DIRK3* (B2) *and the 4-stage DIRK3* (B10) *degenerate to first orders for CFL* < 2*. In the asymptotic limit with* $\epsilon = 10^{-6}$*, all schemes tested are observed to be stable for rather large CFL numbers. The 3-stage DIRK3* (B2) *only has second order convergence. The 4-stage DIRK3* (B10) *displays third order asymptotic convergence for CFL* > 10*, then its error stays the same for CFL ranges from 1 to 7.*

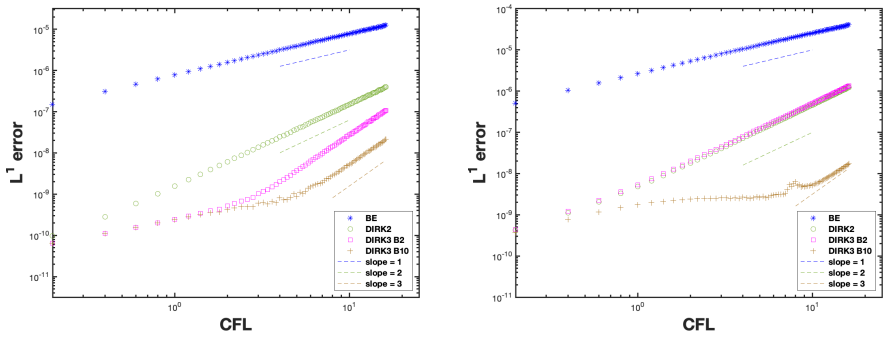

(a) $\epsilon = 10^{-2}$ (b) $\epsilon = 10^{-6}$

FIG. 5.3. *Plots of* L^1 *errors versus CFL on fixed mesh* $N_x = 640$ *for* (5.2) *in* $\epsilon = 10^{-2}, 10^{-6}$ *regimes at* $T = 0.04$*. The reference solutions are obtained from the corresponding numerical solutions with CFL* $= 0.01$*. BE, DIRK2, DIRK3 B2, DIRK3 B10 refer to backward Euler, DIRK2 method* (B1)*, classical 3-stage DIRK3 method* (B2) *and 4-stage DIRK3 method* (B10) *respectively. Line segments of slope 1, 2 and 3 are also provided as references.*

6. Conclusions. In this paper, we study the asymptotic accurate property of the DIRK methods when they are coupled with semi-Lagrangian solvers for stiff hyperbolic relaxation systems and kinetic BGK model. By performing an accuracy analysis in the asymptotic limit of $\epsilon \to 0$, an additional order condition is derived for third order accuracy of DIRK methods in the limiting fluid regime. In additional, linear stability analysis of DIRK schemes is performed on a linear two-velocity model via Fourier analysis, when the spatial operations are kept continuous. Numerical insta-

bilities show up for the limiting fluid regime, with CFL greater than 1. Further study of linear stability of fully discrete DIRK schemes when coupled with discontinuous Galerkin spatial discretization is open and optimization of DIRK methods for better linear and nonlinear stability, are subject to our future work.

Appendix: Butcher Tableaus of DIRK methods. Classical 2-stage DIRK2 in Table B1 and 3-stage DIRK3 methods in Table B2:

$$\begin{array}{c|cc} \nu & \nu & 0 \\ 1 & 1-\nu & \nu \\ \hline & 1-\nu & \nu \end{array}, \qquad \nu = 1-\sqrt{2}/2.$$

TABLE B1

DIRK2.

$$\begin{array}{c|ccc} \gamma & \gamma & & \\ \frac{1+\gamma}{2} & \frac{1-\gamma}{2} & \gamma & \\ 1 & \beta_1 & \beta_2 & \gamma \\ \hline & \beta_1 & \beta_2 & \gamma \end{array}, \qquad \begin{array}{l} \gamma \approx 0.435866521508459, \\ \beta_1 = -\frac{3}{2}\gamma^2 + 4\gamma - \frac{1}{4}, \beta_2 = \frac{3}{2}\gamma^2 - \\ 5\gamma + \frac{5}{4} \end{array}$$

TABLE B2

3-stage DIRK3.

Proposed DIRK3 methods in Table B3-B10 satisfying the order conditions $G_s = 1/6$ in Theorem 3.6:

1.482285978970554	1.482285978970554			
0.840649305846235	-0.6416366731243188	1.482285978970554		
0.369773737448817	0.849139645385794	-1.961651886907531	1.482285978970554	
1	-0.1539440520308502	-1.343634476018696	1.015292549078992	1.482285978970554
	-0.1539440520308502	-1.343634476018696	1.015292549078992	1.482285978970554

TABLE B3

4-stage DIRK3

REFERENCES

[1] G. ALBI, G. DIMARCO, AND L. PARESCHI, *Implicit-explicit multistep methods for hyperbolic systems with multiscale relaxation*, preprint, (2019).

0.1376586577601238	0.1376586577601238			
0.5601286538192144	0.4224699960590905	0.13765865776012381		
0.6273053597634042	0.3693098698936377	0.1203368321096427	0.1376586577601238	
1	0.330756291090243	0.2479472066914047	0.2836378444582285	0.1376586577601238
	0.330756291090243	0.2479472066914047	0.2836378444582285	0.1376586577601238

TABLE B4

4-stage DIRK3

4.025563222205342	4.025563222205342			
2.891263084714272	-1.13430013749107	4.025563222205342		
1.871613091897857	0.8450375691764959	-2.998987699483981	4.025563222205342	
1	-1.33950660036402	4.925563641076701	-6.611620262918024	4.025563222205342
	-1.33950660036402	4.925563641076701	-6.611620262918024	4.025563222205342

TABLE B5

4-stage DIRK3

[2] U. ASCHER, S. RUUTH, AND B. WETTON, *Implicit-explicit methods for time-dependent partial differential equations*, SIAM J. Numer. Anal., 32 (1995), pp. 797–823.

[3] U. M. ASCHER, S. J. RUUTH, AND R. J. SPITERI, *Implicit-explicit Runge-Kutta methods for time-dependent partial differential equations*, Applied Numerical Mathematics, 25 (1997), pp. 151–167.

[4] P. L. BHATNAGAR, E. P. GROSS, AND M. KROOK, *A model for collision processes in gases. I. Small amplitude processes in charged and neutral one-component systems*, Physical review, 94 (1954), p. 511.

[5] S. BOSCARINO, S.-Y. CHO, G. RUSSO, AND S.-B. YUN, *High order conservative Semi-Lagrangian scheme for the BGK model of the Boltzmann equation*, arXiv preprint arXiv:1905.03660, (2019).

[6] J. C. BUTCHER, *The numerical analysis of ordinary differential equations: Runge-Kutta and general linear methods*, Wiley-Interscience, 1987.

[7] M. CALVO, J. DE FRUTOS, AND J. NOVO, *Linearly implicit Runge–Kutta methods for advection–reaction–diffusion equations*, Applied Numerical Mathematics, 37 (2001), pp. 535–549.

[8] C. CERCIGNANI, *The Boltzmann equation and its applications. 1988*, Applied Mathematical Sciences, (1988).

[9] C. CERCIGNANI, *Rarefied gas dynamics: from basic concepts to actual calculations*, vol. 21, Cambridge University Press, 2000.

[10] C. CERCIGNANI ET AL., *Mathematical methods in kinetic theory*, Springer, 1969.

[11] S. CHAPMAN, T. G. COWLING, AND D. BURNETT, *The mathematical theory of non-uniform gases: an account of the kinetic theory of viscosity, thermal conduction and diffusion in gases*, Cambridge university press, 1990.

[12] G. DIMARCO AND L. PARESCHI, *Exponential Runge-Kutta methods for stiff kinetic equations*, SIAM J. Numer. Anal., 49 (2011), pp. 2057–2077.

[13] G. DIMARCO AND L. PARESCHI, *Asymptotic preserving implicit-explicit Runge–Kutta methods for nonlinear kinetic equations*, SIAM Journal on Numerical Analysis, 51 (2013), pp. 1064–1087.

$\frac{1}{2}$	$\frac{1}{2}$			
$\frac{1}{4}$	$-\frac{1}{4}$	$\frac{1}{2}$		
$\frac{3}{2}$	-1	2	$\frac{1}{2}$	
1	$-\frac{1}{12}$	$\frac{2}{3}$	$-\frac{1}{12}$	$\frac{1}{2}$
	$-\frac{1}{12}$	$\frac{2}{3}$	$-\frac{1}{12}$	$\frac{1}{2}$

TABLE B6

4-*stage DIRK3*

0.153198102889014	0.153198102889014			
0.601231025797714	0.448032922908699	0.153198102889014		
0.174793845034303	0.0	0.021595742145288	0.153198102889014	
1	0.0	0.466155735240408	0.380646161870577	0.153198102889014
	0.0	0.466155735240408	0.380646161870577	0.153198102889014

TABLE B7

4-*stage DIRK3*

0.193031472980198	0.193031472980198			
0.087206714188908	-0.105824758791290	0.193031472980198		
0.479857673328132	0.0	0.286826200347934	0.193031472980198	
1	0.0	0.204409312996206	0.602559214023597	0.193031472980198
	0.0	0.204409312996206	0.602559214023597	0.193031472980198

TABLE B8

4-*stage DIRK3*

0.127224858518235	0.127224858518235			
0.331603489550386	0.204378631032151	0.127224858518235		
0.989624239986447	0.0	0.862399381468212	0.127224858518235	
1	0.0	0.746092420734223	0.126682720747542	0.127224858518235
	0.0	0.746092420734223	0.126682720747542	0.127224858518235

TABLE B9

4-*stage DIRK3*

$\frac{1}{4}$	$\frac{1}{4}$			
$\frac{11}{28}$	$\frac{1}{7}$	$\frac{1}{4}$		
$\frac{1}{3}$	$\frac{61}{144}$	$-\frac{49}{144}$	$\frac{1}{4}$	
1	0	0	$\frac{3}{4}$	$\frac{1}{4}$
	0	0	$\frac{3}{4}$	$\frac{1}{4}$

TABLE B10

4-*stage DIRK3*

[14] G. DIMARCO AND L. PARESCHI, *Implicit-explicit linear multistep methods for stiff kinetic equations*, SIAM J. Numer. Anal., 55 (2017), pp. 664–690.

[15] M. DING, J.-M. QIU, AND R. SHU, *Semi-Lagrangian nodal discontinuous Galerkin method for the BGK Model*, 2021, https://arxiv.org/abs/2105.02421.

[16] F. FILBET AND S. JIN, *A class of asymptotic-preserving schemes for kinetic equations and related problems with stiff sources*, J. Comput. Phys., 229 (2010), pp. 7625–7648.

[17] M. GROPPI, G. RUSSO, AND G. STRACQUADANIO, *High order semi-Lagrangian methods for the BGK equation*, arXiv preprint arXiv:1411.7929, (2014).

[18] J. HU AND R. SHU, *A second-order asymptotic-preserving and positivity-preserving exponential Runge-Kutta method for a class of stiff kinetic equations*, arXiv preprint arXiv:1807.03728, (2018).

[19] J. HU AND R. SHU, *On the uniform accuracy of implicit-explicit backward differentiation formulas (IMEX-BDF) for stiff hyperbolic relaxation systems and kinetic equations*, arXiv preprint arXiv:1912.00559, (2019).

[20] J. HU, R. SHU, AND X. ZHANG, *Asymptotic-preserving and positivity-preserving implicit-explicit schemes for the stiff BGK equation*, SIAM Journal on Numerical Analysis, 56 (2018), pp. 942–973.

[21] J. HUANG AND C.-W. SHU, *Bound-preserving modified exponential Runge-Kutta discontinuous Galerkin methods for scalar hyperbolic equations with stiff source terms*, J. Comput. Phys., 361 (2018), pp. 111–135.

[22] W. HUNDSDORFER AND S. RUUTH, *IMEX extensions of linear multistep methods with general monotoncity and boundedness properties*, J. Comput. Phys., 225 (2007), pp. 2016–2042.

[23] S. JIN, *Runge-Kutta methods for hyperbolic conservation laws with stiff relaxation terms*, J. Comput. Phys., 122 (1995), pp. 51–67.

[24] S. JIN, *Efficient asymptotic-preserving (AP) schemes for some multiscale kinetic equations*, SIAM J. Sci. Comput., 21 (1999), pp. 441–454.

[25] S. JIN AND Z. P. XIN, *The relaxation schemes for systems of conservation laws in arbitrary space dimensions*, Commun. Pure Appl. Math., 48 (1995), pp. 235–276.

[26] Q. LI AND L. PARESCHI, *Exponential Runge-Kutta for the inhomogeneous Boltzmann equations with high order of accuracy*, J. Comput. Phys., 259 (2014), pp. 402–420.

[27] S.-J. LIN AND R. B. ROOD, *Multidimensional flux-form semi-Lagrangian transport schemes*, Monthly Weather Review, 124 (1996), pp. 2046–2070.

[28] L. PARESCHI AND G. RUSSO, *Implicit–explicit Runge–Kutta schemes and applications to hyperbolic systems with relaxation*, Journal of Scientific computing, 25 (2005), pp. 129–155.

[29] S. PIERACCINI AND G. PUPPO, *Implicit–explicit schemes for BGK kinetic equations*, Journal of Scientific Computing, 32 (2007), pp. 1–28.

[30] P. SANTAGATI AND G. RUSSO, *A New Class of Conservative Large Time Step Methods for the BGK Models of the Boltzmann Equation*, arXiv preprint arXiv:1103.5247, (2011).

[31] C.-W. SHU AND S. OSHER, *Efficient implementation of essentially non-oscillatory shock-capturing schemes*, Journal of computational physics, 77 (1988), pp. 439–471.

[32] E. SONNENDRÜCKER, J. ROCHE, P. BERTRAND, AND A. GHIZZO, *The semi-Lagrangian method for the numerical resolution of the Vlasov equation*, Journal of computational physics, 149 (1999), pp. 201–220.

[33] A. STANIFORTH AND J. CÔTÉ, *Semi-Lagrangian integration schemes for atmospheric models-A review*, Monthly weather review, 119 (1991), pp. 2206–2223.

[34] G. WANNER AND E. HAIRER, *Solving ordinary differential equations II*, vol. 375, Springer Berlin Heidelberg, 1996.